

# Future Measurements of Deeply Virtual Compton Scattering at HERMES

V. A. Korotkov<sup>a,b</sup> and W.-D. Nowak<sup>a</sup>

<sup>a</sup> DESY Zeuthen, D-15735 Zeuthen, Germany

<sup>b</sup> IHEP, RU-142284 Protvino, Russia

## Abstract

Prospects for future measurements of Deeply Virtual Compton Scattering at HERMES are studied using different simple models for parameterizations of generalized parton distributions (GPDs). Measurements of the lepton charge and lepton beam helicity asymmetry will yield important input for theoretical models towards the future extraction of GPDs.

## 1 Introduction

The study of hard exclusive processes in the Bjorken limit is now considered as a promising tool to gain new insight into details of the nucleon structure that cannot be studied with inclusive deep inelastic scattering (DIS). A unified theoretical description of hard exclusive and inclusive processes has been obtained through the formalism of generalized parton distributions [1, 2, 3] (see recent reviews in Ref.s [4, 13]) which are also called skewed, off-forward or non-forward parton distributions.

An ordinary parton distribution represents the probability to find a parton with a specified longitudinal momentum fraction  $x$  in the fast moving hadron and thus is summing over all partonic configurations containing such a parton. In contrast, GPDs represent the interference of two different wave functions, one with a parton having momentum fraction  $x + \xi$  and another one with a parton having momentum fraction  $x - \xi$ . GPDs, besides the longitudinal momentum fraction variables  $x$  and  $\xi$  (called skewedness parameter), depend on a third independent variable, the momentum transfer  $\Delta^2 = (p - p')^2$  between initial and final nucleon states with momenta  $p$  and  $p'$ , respectively.

There are four different types of quark GPDs contributing to the simplest hard exclusive process: Deeply Virtual Compton Scattering (DVCS),  $ep \rightarrow ep\gamma$ . In the unpolarized distributions,  $H^q(x, \xi, \Delta^2)$  and  $E^q(x, \xi, \Delta^2)$ , the quark helicities are summed over. The polarized distributions,  $\widetilde{H}^q(x, \xi, \Delta^2)$  and  $\widetilde{E}^q(x, \xi, \Delta^2)$ , are responsible for the differences between right- and left-handed quarks.

The generalized parton distributions combine the characters of both the ordinary parton distributions and of nucleon form factors. On the one hand, in the limit  $\Delta^2 \rightarrow 0$ ,  $\xi \rightarrow 0$  holds

$$H^q(x, 0, 0) = q(x), \quad \widetilde{H}^q(x, 0, 0) = \Delta q(x), \quad (1)$$

where  $q(x)$  and  $\Delta q(x)$  are the ordinary quark number density and quark helicity distributions. On the other hand, the first moment of GPDs must satisfy the following sum rules,

$$\begin{aligned}
\int_{-1}^1 dx H^q(x, \xi, \Delta^2) &= F_1^q(\Delta^2) , \\
\int_{-1}^1 dx E^q(x, \xi, \Delta^2) &= F_2^q(\Delta^2) , \\
\int_{-1}^1 dx \widetilde{H}^q(x, \xi, \Delta^2) &= g_A^q(\Delta^2) , \\
\int_{-1}^1 dx \widetilde{E}^q(x, \xi, \Delta^2) &= h_A^q(\Delta^2) ,
\end{aligned} \tag{2}$$

where  $F_1^q(\Delta^2)$  and  $F_2^q(\Delta^2)$  are the Dirac and Pauli form factors and  $g_A^q(\Delta^2)$  and  $h_A^q(\Delta^2)$  are the axial-vector and pseudo-scalar form factors, respectively.

In the above formulae the variable  $x$  is defined in the range  $(-1, +1)$  and negative values of it correspond to anti-quark distributions in the following manner:

$$q(-x) = -\bar{q}(x), \quad \Delta q(-x) = \Delta \bar{q}(x). \tag{3}$$

Two different regions exist for GPDs with respect to the variables  $x$  and  $\xi$ . For  $|x| > \xi$  the GPDs are the generalizations of the ordinary parton distributions, while for  $|x| < \xi$  the GPDs behave like meson distribution amplitudes.

The recent strong interest in GPDs was stimulated by the finding of Ji [2] that the second moment of the unpolarized GPDs at  $\Delta^2 = 0$  is relevant to the spin structure of the nucleon since it determines the total quark angular momentum:

$$J_q = \frac{1}{2} \int_{-1}^{+1} dx x \left[ H^q(x, \xi, \Delta^2 = 0) + E^q(x, \xi, \Delta^2 = 0) \right]. \tag{4}$$

The total quark angular momentum  $J_q$  decomposes as

$$J_q = \frac{1}{2} \Delta \Sigma + L_q, \tag{5}$$

where  $\Delta \Sigma/2$  and  $L_q$  denote quark spin and orbital angular momentum, respectively. As  $\Delta \Sigma$  is measured through polarized DIS experiments, a measurement of  $J_q$  through the sum rule Eq. (4) in terms of GPDs provides a model-independent way to determine the contribution of the quark orbital momentum to the nucleon spin. Eventually even the contribution of the total gluon angular momentum  $J_g$  may become accessible through

$$\frac{1}{2} = J_q + J_g. \tag{6}$$

First measurements of the DVCS lepton helicity asymmetry have been accomplished recently by HERMES [5] at 27.5 GeV and by CLAS [6] at 4.25 GeV. Several plans exist for further measurements of DVCS and of other hard exclusive reactions to accomplish a first insight into GPDs. At HERMES, an upgrade of the spectrometer with a recoil detector [7] will significantly improve the separation of exclusive events. The DVCS process has also been observed in  $e^+p$  collider experiments at DESY by ZEUS [8] and H1 [9]. The DVCS cross section was measured and compared to the QCD-based predictions. Measurements of the lepton beam helicity asymmetry by H1 and ZEUS will become possible in the near future when longitudinally polarized leptons will be made available also to the collider experiments at HERA.

The main aim of this paper is the evaluation of the anticipated statistical accuracy for future measurements of DVCS asymmetries at HERMES upgraded with the recoil detector. In section 2 of the paper different versions of GPD parameterizations are discussed. The third section deals with the assessment of the expected size of the asymmetries, based upon different GPD parameterizations, and with the evaluation of their projected statistical accuracy. Finally, the conclusions of the paper are presented.

## 2 Parameterization of Generalized Parton Distributions

Two examples of GPD calculations are presently known in the literature. While bag model calculations [10] show a weak dependence of the distributions on the skewedness parameter, chiral quark soliton model calculations [11], in contrast, show a strong dependence on  $\xi$ . The common approach at the moment is to use a guess that satisfies general constraints on GPDs known from theory. This paper basically follows the ansatz proposed in Ref.s [12, 13]. Here, the dependence of the GPDs on  $\Delta^2$  is taken in a factorized form with respect to the other variables whereby satisfying Eq.(2). Any scale dependence of the GPDs is neglected.

In the simplest approach GPDs can be assumed to be independent of the skewedness parameter  $\xi$ . In the following, only  $u$ - and  $d$ -quark GPDs are considered to be non-zero. The function  $H$ , for example, is written as a product of an ordinary quark distribution function and a form factor

$$\begin{aligned} H^u(x, \xi, \Delta^2) &= u(x) F_1^u(\Delta^2) / 2, \\ H^d(x, \xi, \Delta^2) &= d(x) F_1^d(\Delta^2). \end{aligned} \quad (7)$$

Here  $u(x)$  and  $d(x)$  are the unpolarized quark distributions and  $F_1^{u(d)}(\Delta^2)$  are defined through the electro-magnetic form factors of proton and neutron:

$$F_1^u = 2F_1^p + F_1^n, \quad F_1^d = F_1^p + 2F_1^n. \quad (8)$$

In the same context, the function  $\widetilde{H}$  is written to be related to quark helicity distributions and axial-vector form factors:

$$\begin{aligned} \widetilde{H}^u(x, \xi, \Delta^2) &= \Delta u_V(x) g_A^u(\Delta^2) / g_A^u(0), \\ \widetilde{H}^d(x, \xi, \Delta^2) &= \Delta d_V(x) g_A^d(\Delta^2) / g_A^d(0), \end{aligned} \quad (9)$$

where  $g_A^u = \frac{1}{2}g_A + \frac{1}{2}g_A^0$ ,  $g_A^d = -\frac{1}{2}g_A + \frac{1}{2}g_A^0$  and  $g_A^0 = \frac{3}{5}g_A$ .

The functions  $E$  and  $\widetilde{E}$  have no definite limit at  $\Delta^2 \rightarrow 0$ ,  $\xi \rightarrow 0$ , as it exists for the functions  $H$  and  $\widetilde{H}$  (cf. Eq. (1)). In absence of any other guide the ansatz for  $E$  is chosen in a form analogous to the function  $H$ :

$$\begin{aligned} E^u(x, \xi, \Delta^2) &= u(x) F_2^u(\Delta^2) / 2, \\ E^d(x, \xi, \Delta^2) &= d(x) F_2^d(\Delta^2), \end{aligned} \quad (10)$$

where  $F_2^{u(d)}$  is defined in the same way as  $F_1^{u(d)}$  in Eq. (8).

The function  $\widetilde{E}$  is modelled to be due to the pion pole:

$$\widetilde{E}^u(x, \xi, \Delta^2) = -\widetilde{E}^d(x, \xi, \Delta^2) = \frac{1}{2} \widetilde{E}_{\pi\text{-pole}}(x, \xi, \Delta^2), \quad (11)$$

$$\widetilde{E}_{\pi\text{-pole}}(x, \xi, \Delta^2) = \theta(-\xi \leq x \leq \xi) h_A(\Delta^2) \frac{1}{\xi} \Phi\left(\frac{x}{\xi}\right), \quad (12)$$

where  $\Phi(z) = 3/4(1 - z^2)$  is the pion distribution amplitude,  $h_A(\Delta^2) = \frac{4M^2 g_A}{m_\pi^2 - \Delta^2}$ , and  $\theta(x)$  is the usual step function.

To introduce, as a next step, a dependence of the GPDs on the skewedness parameter  $\xi$ , the double-distribution formalism [1, 3] can be used. In this model, the  $\Delta^2$ -independent part of the function  $H$  can be written in the following form

$$H_{DD}^q(x, \xi) = \int_{-1}^1 dy \int_{-1+|y|}^{1-|y|} dt \delta(x - y - t\xi) h(y, t) q(y). \quad (13)$$

Here  $q(y)$  is the ordinary quark distribution and  $h(y, t)$  is the so-called profile function:

$$h(y, t) = \frac{\Gamma(2b+2)}{2^{2b+1}\Gamma^2(b+1)} \frac{[(1-|y|)^2 - t^2]^b}{(1-|y|)^{2b+1}}, \quad (14)$$

with  $b$  as a free parameter and  $b \rightarrow \infty$  corresponding to the skewedness-independent parameterization. Analogous expressions can be written for the functions  $\widetilde{H}$  and  $E$ .

The functions  $H$  and  $E$  in the form of double distributions lack the correct polynomiality properties of GPDs. However, they can be restored by introducing the so-called  $D$ -term [14]. The  $D$ -term contribution has different sign for  $H$  and  $E$  and hence cancels in Ji's angular momentum sum rule Eq. (4). The full model expressions for the GPDs therefore have the following form:

$$\begin{aligned} H^q(x, \xi) &= H_{DD}^q(x, \xi) + \theta(\xi - |x|) \frac{1}{N_f} D\left(\frac{x}{\xi}\right), \\ E^q(x, \xi) &= E_{DD}^q(x, \xi) - \theta(\xi - |x|) \frac{1}{N_f} D\left(\frac{x}{\xi}\right), \end{aligned} \quad (15)$$

where  $N_f = 3$  is the number of active flavors. The parameterization of the  $D$ -term is taken in a form that follows from chiral quark soliton model calculations [15]. For more details on possible GPD parameterizations and their discussion we refer to Ref.s [12, 13].

Quark number density and quark helicity distributions  $q(x)$  and  $\Delta q(x)$ , respectively, were used in the parameterizations of Ref. [16] (at  $Q^2 = 2 \text{ GeV}^2$ ) and Ref. [17] (at  $Q^2 = 1 \text{ GeV}^2$ ).

In the projections described below five different versions of GPD parameterizations were included:

- (A)  $H(x, \xi)$ ,  $\widetilde{H}(x, \xi)$ , and  $E(x, \xi)$  are skewedness independent and given by Eq.s (7), (9), and (10), respectively.
- (B) The skewedness dependence of  $H(x, \xi)$ ,  $\widetilde{H}(x, \xi)$ , and  $E(x, \xi)$  is generated through the double-distribution formalism Eq.s (13) and (14) with the parameter  $b = 1$ .
- (C) same as (B), but with the parameter  $b = 3$ .
- (D) same as (B), but the contribution of the  $D$ -term to  $H(x, \xi)$  and  $E(x, \xi)$  is included additionally, according to Eq.(15).
- (E) same as (D), but with the parameter  $b = 3$ .

For  $\widetilde{E}(x, \xi)$  the pion pole expression Eq. (11) is used for all versions of GPDs.

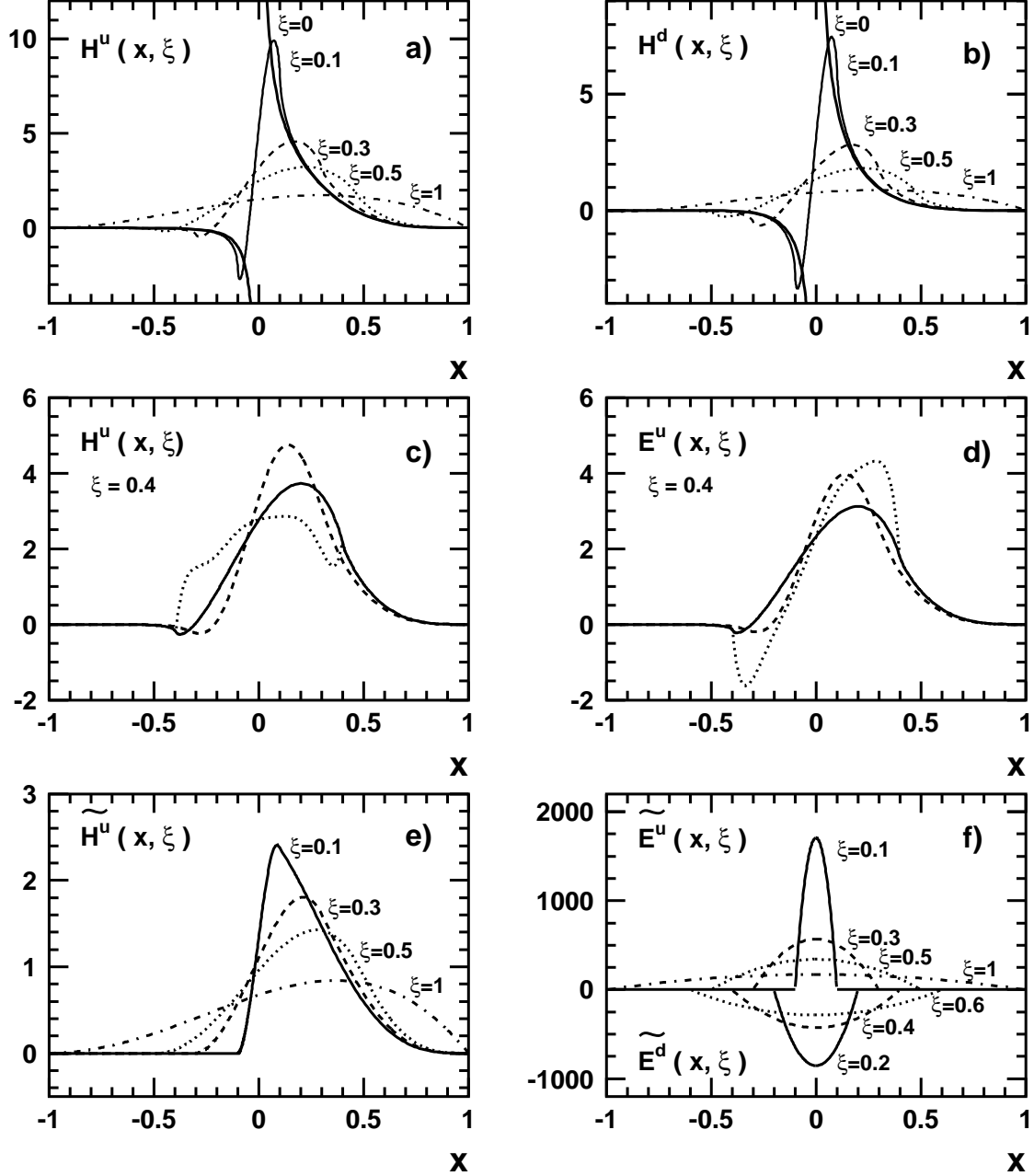


Figure 1: *Illustration of the  $x$ -behaviour of various generalized parton distributions for different values of the skewedness parameter  $\xi$  (at  $\Delta^2 = 0$ ). For explanations see text.*

The dependences of the GPDs on the variables  $x$  and  $\xi$  (at  $\Delta^2 = 0$ ), obtained from these five different parameterizations, are displayed for a few examples in fig. 1. Panels a) and b) show the GPD  $H$  in version (B) for different values of  $\xi$ , compared between  $u$ - and  $d$ -quark. Panels c) and d) show the unpolarized  $u$ -quark GPDs  $H$  and  $E$  at fixed  $\xi = 0.4$ , compared between different versions: (B) as solid line, (C) as dashed line and (D) as dotted line. Panels e) and f) show the polarized  $u$ -quark GPDs  $\tilde{H}$  and  $\tilde{E}$  in version (B) compared for different values of  $\xi$ . Although  $\tilde{E}$  does not appear in the DVCS asymmetries (see below), its  $u$ - vs.  $d$ -quark comparison is shown, as well. By definition  $\tilde{E}$  is large at  $\Delta^2 = 0$  (see Eq. (11)).

### 3 Deeply Virtual Compton Scattering

In the Bjorken limit, DVCS is dominated by the handbag diagram (fig. 2) and its amplitude can be factorized into a soft part described by GPDs and a hard part representing a parton process calculable in perturbative QCD. In this limit the skewedness parameter  $\xi$  can be related to the Bjorken variable  $x_B$ :

$$\xi = \frac{x_B/2}{1 - x_B/2} \quad (16)$$

The same final state,  $ep\gamma$ , can also be produced via the Bethe-Heitler (BH) process in which an electron scatters elastically off the target proton and the initial or final state electron radiates a real photon. The cross section of this process can be calculated exactly once the Dirac and Pauli nucleon form-factors are known. On the one hand, the BH process constitutes the main background to DVCS, on the other hand their interference opens the unique opportunity for independent measurements of the real and imaginary parts of a certain DVCS amplitude combination (see below).

The cross-section of the DVCS process and its interference with the BH process has been considered in a number of papers [2, 3]. The kinematic configuration of the process  $ep \rightarrow ep\gamma$  is shown in fig. 3. Here  $\phi_\gamma$  describes the azimuthal orientation of the production plane (comprising  $\gamma^*$ ,  $\gamma$  and  $p$ ) relative to the scattering plane (comprising initial and final lepton, as well as the virtual photon). The laboratory polar angle between virtual and real photon is denoted by  $\theta_{\gamma\gamma^*}$ . In-plane (i.e.  $\phi_\gamma = 0$ ) differential cross-sections for DVCS, BH and total  $\gamma$  production in  $e^+p$  interactions at the HERMES energy of  $E_e = 27.5$  GeV were calculated following Ref. [2] and are presented in fig. 4. The DVCS cross-section shows a maximum at  $\Theta_{\gamma\gamma^*} = 0$ , while the BH cross-section has a three-pole structure due to the propagators of the virtual electrons and the virtual photon. It is apparent that at HERMES energies the cross-section of DVCS is smaller than that of BH over practically the entire kinematic region. Therefore measurements of GPDs at HERMES must be based upon the interference between the DVCS and BH processes.

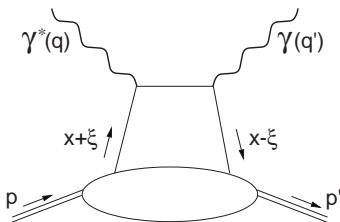


Figure 2: *Leading handbag diagram for DVCS.*

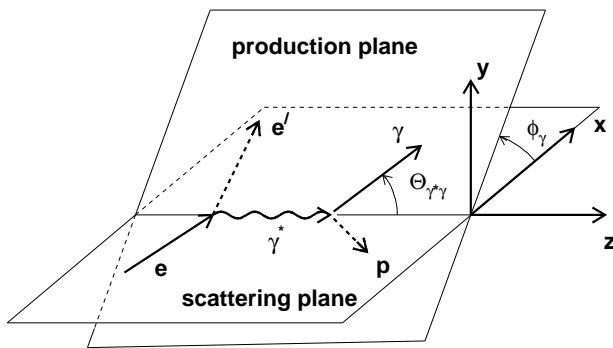


Figure 3: *Kinematic configuration for the process  $ep \rightarrow ep\gamma$ .*

In Ref. [18] amplitudes of DVCS, BH and of the interference terms were calculated at the leading twist-2 level for polarized and unpolarized initial particles. This approach was used to determine the below presented projections for future measurements of DVCS-BH interference effects at HERMES.

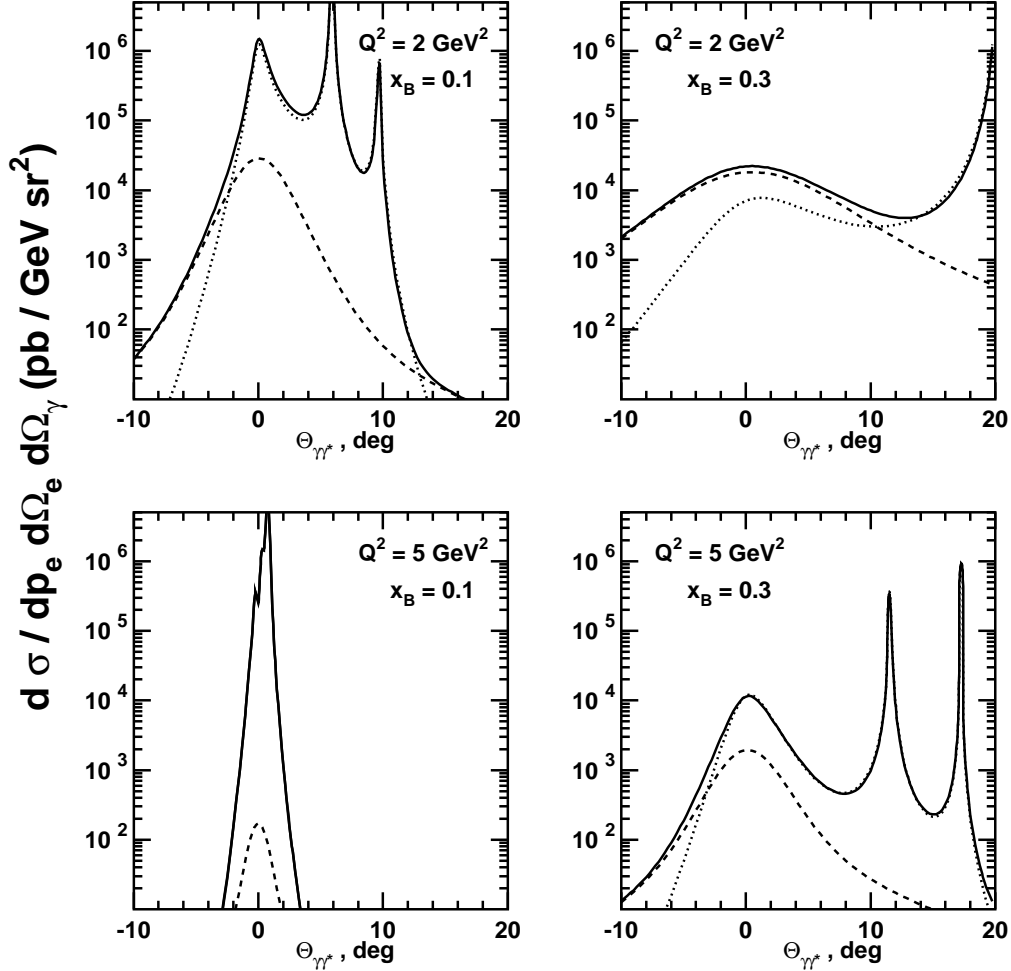


Figure 4: *Illustration of the behaviour of the differential in-plane cross-section as a function of the polar angle between the virtual and the real photon for DVCS (dashed lines), Bethe-Heitler (dotted lines) and total  $\gamma$  production (solid lines) in  $e^+p$  interactions at HERMES energy  $E_e = 27.5$  GeV. Different panels are for different values of  $x_B$  and  $Q^2$ .*

The primary interest of HERMES in the context of the planned recoil detector upgrade lies with measurements using an unpolarized proton target. In this case two different types of experiments are possible that will be giving insight into GPDs:

I) Measurements of the lepton charge asymmetry with unpolarized leptons of either charge:

$$d\Delta\sigma_{ch} \equiv d\sigma(e^+p) - d\sigma(e^-p) \sim \cos(\phi_\gamma) \times \text{Re} \left\{ F_1 \mathcal{H}_1 + \frac{x_B}{2-x_B} (F_1 + F_2) \widetilde{\mathcal{H}}_1 - \frac{\Delta^2}{4M^2} F_2 \mathcal{E}_1 \right\} \quad (17)$$

This asymmetry allows access to the real parts of the DVCS amplitudes  $\mathcal{H}_1$ ,  $\widetilde{\mathcal{H}}_1$ , and  $\mathcal{E}_1$ .

II) Measurements of the beam helicity asymmetry using a polarized positron beam:

$$d\Delta\sigma_{LU} \equiv d\sigma(\vec{e}^+p) - d\sigma(\overleftarrow{e}^+p) \sim \sin(\phi_\gamma) \times \text{Im} \left\{ F_1 \mathcal{H}_1 + \frac{x_B}{2-x_B} (F_1 + F_2) \widetilde{\mathcal{H}}_1 - \frac{\Delta^2}{4M^2} F_2 \mathcal{E}_1 \right\} \quad (18)$$

This asymmetry allows access to the imaginary parts of the same amplitudes.

The imaginary and real parts of the DVCS amplitudes  $\mathcal{H}_1$  and  $\widetilde{\mathcal{H}}_1$  are related to the GPDs  $H$  and  $\widetilde{H}$  as follows:

$$\begin{aligned}
\text{Im } \mathcal{H}_1 &= -\pi \sum_q e_q^2 (H(\xi, \xi, \Delta^2) - H(-\xi, \xi, \Delta^2)), \\
\text{Im } \widetilde{\mathcal{H}}_1 &= -\pi \sum_q e_q^2 (\widetilde{H}(\xi, \xi, \Delta^2) + \widetilde{H}(-\xi, \xi, \Delta^2)), \\
\text{Re } \mathcal{H}_1 &= \sum_q e_q^2 \left[ P \int_{-1}^{+1} H(x, \xi, \Delta^2) \left( \frac{1}{x - \xi} + \frac{1}{x + \xi} \right) dx \right], \\
\text{Re } \widetilde{\mathcal{H}}_1 &= \sum_q e_q^2 \left[ P \int_{-1}^{+1} \widetilde{H}(x, \xi, \Delta^2) \left( \frac{1}{x - \xi} - \frac{1}{x + \xi} \right) dx \right], \tag{19}
\end{aligned}$$

where  $P$  denotes Cauchy's principal value. The DVCS amplitudes  $\mathcal{E}_1$  and  $\widetilde{\mathcal{E}}_1$  can be expressed through  $E$  and  $\widetilde{E}$  analogously.

Projections for statistical accuracies attainable in measurements of the lepton charge and lepton beam helicity asymmetry at HERMES were calculated for an integrated luminosity of  $2 \text{ fb}^{-1}$  [7] which corresponds to the expected value for one year of data taking. The HERMES geometrical acceptance for the detection of the scattered electron, the photon and the recoil proton was taken into account. The following kinematic cuts<sup>1</sup> were applied:  $E_e > 3.5 \text{ GeV}$ ,  $W^2 > 4 \text{ GeV}^2$ ,  $Q^2 > 1 \text{ GeV}^2$ ,  $E_\gamma > 1 \text{ GeV}$ ,  $P_p > 0.2 \text{ GeV}$ ,  $0.35 < \theta_p^{lab} < 1.35 \text{ rad}$ , and  $15 < \Theta_{\gamma\gamma^*} < 70 \text{ mrad}$ .

To calculate the asymmetries Eq.s (17) and (18) the 5-fold differential cross-section has to be integrated over the appropriate kinematic region accounting for the HERMES geometrical acceptance:

$$\frac{d\sigma}{d\phi_\gamma} = \int \frac{d^5\sigma}{dx dQ^2 d|\Delta^2| d\phi_\gamma d\phi_{el}} dx dQ^2 d|\Delta^2| d\phi_\gamma d\phi_{el},$$

where  $\phi_{el}$  is the azimuthal angle of the scattered electron. It is appropriate to define differences and sums of certain cross-sections:

$$\begin{aligned}
\frac{d\Delta\sigma_{ch}}{d\phi_\gamma} &= \frac{d\sigma(e^+p)}{d\phi_\gamma} - \frac{d\sigma(e^-p)}{d\phi_\gamma}, \\
\frac{d\Sigma\sigma_{ch}}{d\phi_\gamma} &= \frac{d\sigma(e^+p)}{d\phi_\gamma} + \frac{d\sigma(e^-p)}{d\phi_\gamma}, \\
\frac{d\Delta\sigma_{LU}}{d\phi_\gamma} &= \frac{d\sigma(e^\uparrow p)}{d\phi_\gamma} - \frac{d\sigma(e^\downarrow p)}{d\phi_\gamma}, \\
\frac{d\Sigma\sigma_{LU}}{d\phi_\gamma} &= \frac{d\sigma(e^\uparrow p)}{d\phi_\gamma} + \frac{d\sigma(e^\downarrow p)}{d\phi_\gamma}. \tag{20}
\end{aligned}$$

Using these definitions the  $\phi$ -dependence of the the lepton charge asymmetry reads

$$A_{ch}(\phi) = \frac{\int_{\phi-\Delta\phi}^{\phi+\Delta\phi} d\phi d\Delta\sigma_{ch}/d\phi}{\int_{\phi-\Delta\phi}^{\phi+\Delta\phi} d\phi d\Sigma\sigma_{ch}/d\phi}, \tag{21}$$

---

<sup>1</sup>Here  $E_e$  and  $E_\gamma$  are the energy of the incoming electron and the outgoing photon, respectively, while  $P_p$  is the momentum of the outgoing proton. The standard DIS variables  $Q^2$  and  $W^2$  describe the four-momentum transfer and the energy of the  $\gamma^*p$  system, respectively. The laboratory polar angle of the outgoing proton is given by  $\theta_p^{lab}$ .



while an integrated lepton charge asymmetry can be defined by forming the difference between two integrals over appropriately defined ‘halves’ of the  $\phi$ -distribution:

$$\tilde{A}_{ch} = \frac{\int_{-\pi/2}^{\pi/2} d\phi d\Delta\sigma_{ch}/d\phi - \int_{\pi/2}^{3\pi/2} d\phi d\Delta\sigma_{ch}/d\phi}{\int_0^{2\pi} d\phi d\Sigma\sigma_{ch}/d\phi}. \quad (22)$$

Analogously the  $\phi$ -dependent and an integrated lepton beam helicity asymmetry, respectively, are defined as follows:

$$A_{LU}(\phi) = \frac{\int_{\phi-\Delta\phi}^{\phi+\Delta\phi} d\phi d\Delta\sigma_{LU}/d\phi}{\int_{\phi-\Delta\phi}^{\phi+\Delta\phi} d\phi d\Sigma\sigma_{LU}/d\phi}, \quad (23)$$

$$\tilde{A}_{LU} = \frac{\int_0^{\pi} d\phi d\Delta\sigma_{LU}/d\phi - \int_{\pi}^{2\pi} d\phi d\Delta\sigma_{LU}/d\phi}{\int_0^{2\pi} d\phi d\Sigma\sigma_{LU}/d\phi}. \quad (24)$$

Projections for the statistical accuracy attainable in measuring the lepton charge asymmetry are presented in fig. 5. The results are shown as a function of the azimuthal angle  $\phi_\gamma$  in two regions of  $x_B$ , using different GPD parameterizations. The asymmetry clearly depends on the particular parameterization and can even change its sign in dependence on  $x_b$ . Therefore, in the experiment the asymmetry will have to be studied differentially as much as possible. Apparently, the inclusion of the  $D$ -term leads to essential changes in the asymmetry and future measurements at HERMES may allow to confirm its importance experimentally. In fig. 6 the integrated lepton charge asymmetry  $\tilde{A}_{ch}$  is shown as a function of  $x_B$  and  $\Delta^2$ , based on the GPD parameterization (E). No  $\Delta^2$ -dependence is seen on the basis of the chosen GPD model.

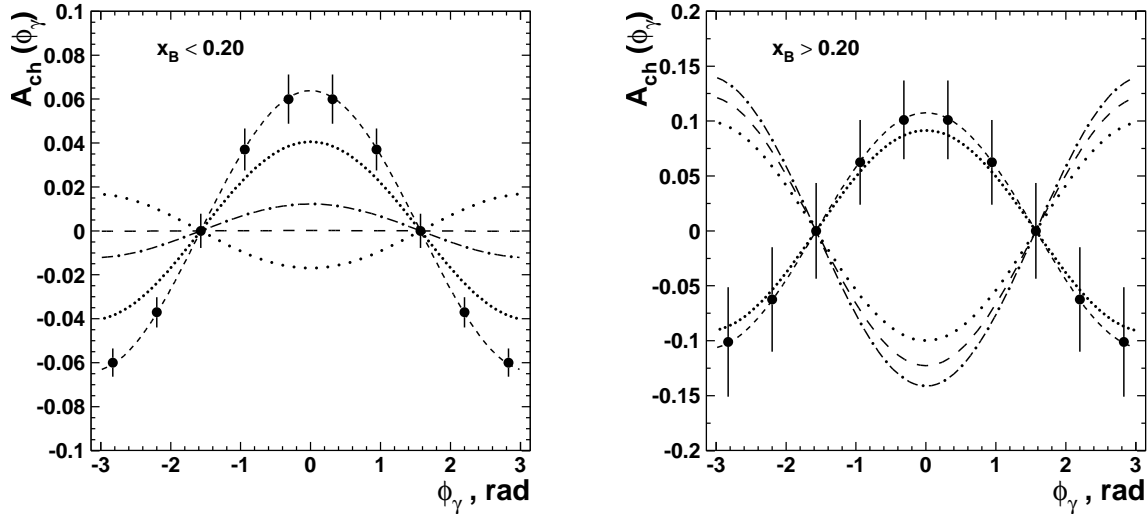


Figure 5: *Projected statistical accuracy for the lepton charge asymmetry Eq. (21) as a function of the azimuthal angle  $\phi_\gamma$  between scattering plane and production plane. Predictions of different GPDs models (see text) are shown in two regions of  $x_B$ . Version (A) - dash-dotted line; version (B) - long-space dotted line; version (C) - long-space dashed line; version (D) - dotted line; version (E) - dashed line.*

Projections for the statistical accuracy attainable in measurements of the helicity asymmetry are presented in fig. 7, as a function of the azimuthal angle  $\phi_\gamma$  (left panel) and as a function of  $x_B$  and  $\Delta^2$  (right panel). As can be seen, the projections of the statistical accuracy promise a

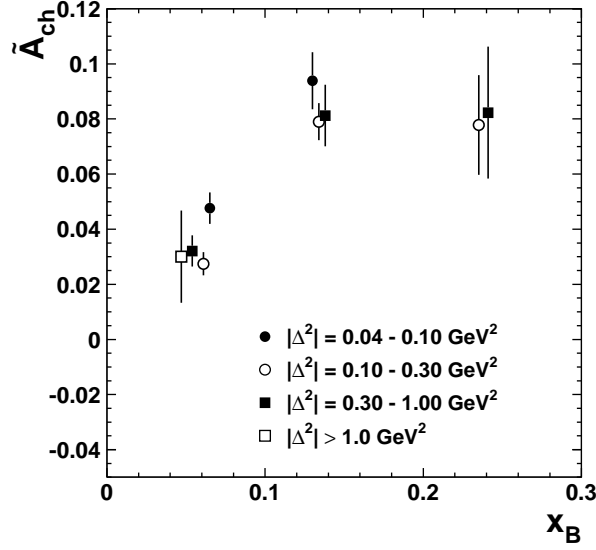


Figure 6: *Projected statistical accuracy for the  $\phi$ -integrated lepton charge asymmetry Eq. (22) as a function of  $x_B$  and  $\Delta^2$  based upon GPD model version (E).*

considerable improvement compared to the present HERMES measurement shown additionally in fig. 7 (left panel). The projected asymmetry changes only slightly in dependence on the GPD parameterizations when the parameter  $b$  of the profile function Eq. (14) varies in the range  $(1 ; \infty)$ . Note that the beam helicity asymmetry is not sensitive to the D-term as it does not contribute to the imaginary parts of DVCS amplitudes.

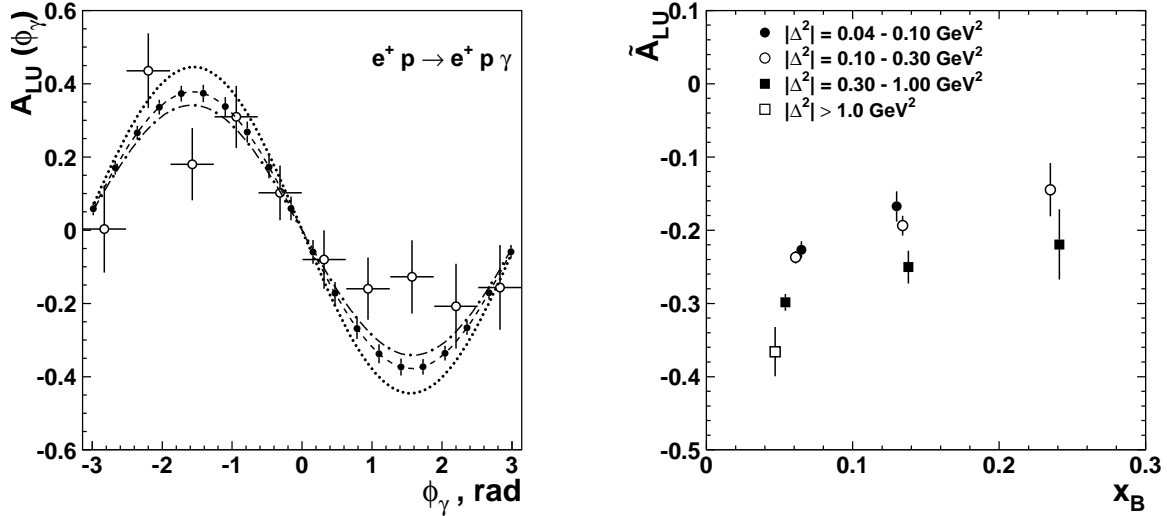


Figure 7: *Projected statistical accuracy for the beam helicity asymmetry Eq.s (23, 24) as a function of the azimuthal angle  $\phi_\gamma$  between scattering plane and production plane (left panel, closed circles) and as a function of  $x_B$  and  $\Delta^2$  (right panel). The line conventions are as in fig. 5. The present measurement of the azimuthal asymmetry by HERMES is shown in the left panel by open circles.*

The considerations presented above are based upon the leading twist-2 level using the amplitudes calculated in Ref. [18]. More elaborate analyses include twist-3 effects [15, 19] and next-to-leading order calculations [20]. Nevertheless, in the present situation where the generalized parton distributions are practically unknown, the approach adopted in this paper appears adequate to evaluate the expected size of the predictions.

It appears worth noting that additional important constraints on GPDs can be expected from the analysis of the same data set by studying hard exclusive production of both pseudo-scalar and vector mesons. As compared to DVCS these processes will provide information on different combinations of generalized parton distributions.

## 4 Conclusions

Expected statistical accuracies have been evaluated for future measurements of Deeply Virtual Compton Scattering with the HERMES spectrometer complemented by a to-be-built recoil detector. Using polarized electrons and positrons of HERA with different helicities, in conjunction with an unpolarized proton target, it becomes possible to measure the lepton charge asymmetry and the lepton beam helicity asymmetry, both induced by the interference of the DVCS and the Bethe-Heitler process. From these asymmetries the real and the imaginary part of a certain DVCS amplitude combination can be determined.

The expected size of the asymmetries has been evaluated using various parameterizations of the underlying generalized parton distributions. A number of different parameterizations has been used to compensate as much as possible for the present poor knowledge on GPDs. The level of the attainable statistical accuracy is mainly determined by the cross section of the Bethe-Heitler process that dominates the reaction  $ep \rightarrow ep\gamma$  at HERMES energies.

It has been shown that the planned measurements of hard exclusive real photon production at HERMES will be of high statistical significance. The envisaged separate results on the real and the imaginary part of a certain DVCS amplitude combination will constitute an important step towards the determination of the generalized parton distributions. The measured constraints will serve as very useful input for the further modelling of generalized parton distributions.

We thank R. Kaiser for careful reading of the manuscript.

## References

- [1] D. Müller et al., Fortsch. Phys. **42**, 101 (1994).
- [2] X. Ji, Phys.Rev.Lett. **78**, 610 (1997); Phys.Rev. **D55**, 7114 (1997).
- [3] A.V. Radyushkin, Phys.Lett. **B380**, 417 (1996); Phys.Rev. **D56**, 5524 (1997).
- [4] A.V. Radyushkin, hep-ph/0101225.
- [5] A. Airapetian et al., hep-ex/0106068
- [6] S. Stepanyan et al., hep-ex/0107043

- [7] A Large Acceptance Recoil Detector for HERMES, DESY PRC 01-01, April 2001.
- [8] P.R.B. Saull, Proc. of the Int. Europhysics Conf. on HEP, Tampere, Finland, 15-21 July 1999, ed. by K. Huitu, H. Kurki-Suonio and J. Maalampi (hep-ex/0003030);  
L. Favart, DIS-2001, Bologna, 27 April - 1 May (hep-ex/0106067).
- [9] C. Adloff et al., DESY 01-093, 2001.
- [10] X. Ji, W. Melnitchouk, X. Song, Phys.Rev. **D56**, 5511 (1997).
- [11] V. Petrov et al., Phys.Rev. **D57**, 4325 (1998).
- [12] M. Vanderhaeghen, P.A.M. Guichon, M. Guidal, Phys.Rev. **D60**, 094017 (1999).
- [13] K. Goeke, M.V. Polyakov, M. Vanderhaeghen, hep-ph/0106012.
- [14] M.V. Polyakov, C. Weiss, Phys.Rev. **D60**, 114017 (1999).
- [15] N. Kivel, M.V. Polyakov, M. Vanderhaeghen, Phys.Rev. **D63**, 114014 (2001).
- [16] A.D. Martin et al., Eur. Phys. J. **C4**, 463 (1998).
- [17] E. Leader, A.V. Sidorov, D.B. Stamenov, Phys.Rev. **D58**, 114028 (1998).
- [18] A.V. Belitsky et al., Nucl.Phys. **B593**, 289 (2001).
- [19] A.V. Belitsky et al., Phys.Lett. **B510**, 117 (2001).
- [20] A. Freund and M. McDermott, hep-ph/0106124.